Tribological behavior of bioactive multi-material structures targeting orthopedic applications

M.M. Costa[a],[*], F. Bartolomeu[a], N. Alves[b], F.S. Silva[a], G. Miranda[a]

[a] Center for Micro-Electro Mechanical Systems (CMEMS-UMinho), University of Minho, Campus de Azurém, 4800-058 Guimarães, Portugal
[b] Centre for Rapid and Sustainable Product Development Polytechnic Institute of Leiria, Rua General Norton de Matos, Apartado 4133, 2411-901 Leiria, Portugal

ABSTRACT

The following study proposes a multi-material solution in which Ti6Al4V cellular structures produced by Selective Laser Melting are impregnated with bioactive materials (hydroxyapatite or β-tricalcium phosphate) using press and sintering technique. To assess the tribological response of these structures, an alumina plate was used as a counterpart in a flat-on-flat reciprocating sliding test. Ti6Al4V cellular structures impregnated with bioactive materials displayed the highest wear resistance when compared with the unreinforced structures. Among the bioactive structures, Ti6Al4V cellular structures impregnated with βTCP were the ones with higher wear resistance, having the lowest weight loss. Hence, these structures are promising multifunctional solutions for load-bearing applications by gathering suitable mechanical properties (strength and stiffness); bioactive properties and in addition an improved wear performance.

1. Introduction

Metallic materials, specially titanium and its alloys, are the first choice of materials for load-bearing orthopedic applications, such as hip or dental implants due to their high mechanical properties (Dantas et al., 2017b, 2017a; Taniguchi et al., 2016).

Among titanium alloys, Ti6Al4V is the most frequently used alloy in orthopedics due to its high strength, biocompatibility, corrosion resistance and lower density among metals (Bartolomeu et al., 2017; Bruschi et al., 2017; Dantas et al., 2017a; Sahoo et al., 2014; Sampaio et al., 2016). In fact, this alloy biocompatibility and corrosion resistance are related with its ability to form an oxide layer on its surface when in contact with atmosphere or an environment with oxygen (Buciumeanu et al., 2018; Massaro et al., 2002; Ratner et al., 1996; Sampaio et al., 2016; Sidambe, 2014). This layer protects the material against corrosion but also promotes an effective cell attachment and growth (Sampaio et al., 2016; Sidambe, 2014). However, despite all its advantages, Ti6Al4V bioinertness can be a drawback to such applications once the adhesion between implant and bone can be quite poor and could lead to implant failure (Aparicio et al., 2011; Horowitz et al., 2009; Pereira et al., 2014; Taniguchi et al., 2016). This bioinertess means that the integration between implant and bone only depends on the tissue integration and regeneration and not the implant itself, which turns interesting the addition of a material that promotes a biological

response and improves implant osseointegration (Aparicio et al., 2011; Ducheyne and Qiu, 1999; Horowitz et al., 2009; Lee et al., 2017; Pereira et al., 2014; Santin and Philips, 2012; Zhang et al., 2016; Zhao et al., 2011).

Bioactive materials like hydroxyapatite (HAp) and β-tricalcium phosphate (βTCP) are materials very similar to the natural apatites of bone, characterized by their excellent biocompatibility, osteoconductivity and cell adhesion and, therefore, interacts with the biological environment, enhancing bone tissue formation and a strong bonding between implant and bone (Dantas et al., 2017a; Ducheyne and Qiu, 1999; Horowitz et al., 2009; Lee et al., 2017; Zhang et al., 2016).

Zhang et. al studied the effect of a bioactive inclusion on porous HAp-Ti alloy composites, regarding mechanical properties and in vitro bioactivity. Results revealed that, besides good mechanical properties, the addition of HAp improves significantly the bioactivity of the material due to the formation of a complete apatite layer formed in these composites (Zhang et al., 2016). Melo-Fonseca et. al, evaluated the influence of multi-material Ti6Al4V cellular structures impregnated with a bioactive bioglass on physical and chemical aspects that drive cellular response, stressing the importance of controlling pH for obtaining a suitable environment for cell growth (Melo-Fonseca et al., 2018). Dantas et al. evaluated the frictional response and surface damage of Ti6Al4V-HAp and Ti6Al4V- βTCP composites, in order to

---

optimize primary stability on prosthesis implantation. In this study, it was concluded that polished bioactive composites promoted an enhanced primary stability when compared with common rough surfaces (Dantas et al., 2017a).

Nowadays Ti6Al4V implants are dense parts, however some endeavors have been made by industry and some research groups to introduce bioactive materials on these implants (Blind et al., 2005; Evis and Doremus, 2007; Karamian et al., 2014; Khandelwal et al., 2013; Ning and Zhou, 2002; Queiroz et al., 2004). Bioactive materials brittle nature makes them not suitable for load bearing applications (Blind et al., 2005; Buciumeanu et al., 2017; Hu et al., 2010; Khandelwal et al., 2013; Ning and Zhou, 2002), in this sense, bioactive coatings are being proposed/developed for Ti6Al4V surfaces (Blind et al., 2005; Evis and Doremus, 2007; Karamian et al., 2014; Khandelwal et al., 2013; Ning and Zhou, 2002; Queiroz et al., 2004), once they allow to combine the titanium alloy suitable mechanical properties and bioactive materials bioactivity. However, upon implantation, coating detachment can occur due to the shear stresses involved on prosthesis insertion, which compromises their function (Miranda et al., 2016; Ryan et al., 2006). Moreover, dense Ti6Al4V implants are not an optimal solution due to its high Young's modulus ($\approx$«110 GPa (Apostu et al., 2017)), that despite being the lower among metals used in implants, is still much higher than that of bone ($\approx$10–30 GPa (Bandyopadhyay et al., 2010)).

Considering the abovementioned, urge the need to find new solutions that effectively approximate the stiffness of the implant to that of bone, by altering implants design.

In this sense, it would be interesting to tailor these implants Young's modulus, to reduce the mismatch between implant and bone. This is possible by introducing controlled porosity, by designing open cellular structures made of Ti6Al4V. These structures, besides decreasing the Young's modulus, are also capable of promoting bone ingrowth, once these structures allow nutrients flow and vascularization to occur (Arabnejad et al., 2016; Tan et al., 2017; Taniguchi et al., 2016). This vascularization will trigger a cascade of biological events that promote new bone formation. In this regard, many studies address the effect of pore size on bone vascularization, concluding that the optimum pore size should range from 100 to 400 μm (Bobyn et al., 1980; Kumar et al., 2016). Moreover, by this approach it is possible to impregnate bioactive materials into the open cells, preventing the bioactive detachment to occur once these materials are imprisoned inside the Ti6Al4V structure by a mechanical interlocking.

Additive manufacturing techniques like selective laser melting (SLM) allows the production of these cellular structures once this technique allows the fabrication of parts with complex geometries that were previously designed in a CAD software. In this process, the CAD data is imported to the SLM machine that will produce the final part in a layer-by-layer process by melting successive layers of powder that are scanned by a laser source (Bartolomeu et al., 2017; Sidambe, 2014; Van Hooreweder et al., 2017). To introduce the bioactive materials into these structures, press and sintering is a suitable powder metallurgy

technique once it forces the bioactive powders to impregnate the open cells, being afterwards sintered.

The present study proposes a novel solution targeting load-bearing applications that allows obtaining the necessary strength and adequate stiffness while introducing bioactivity to enhance implant performance. However, implants performance also depends on the tribological behavior of the final component, which, in fact, is quite poor for Ti6Al4V alloy (Bruschi et al., 2017; Buciumeanu et al., 2018; Dantas et al., 2017b). The corrosive medium present in the human body allied to the poor wear resistance of this material can potentiate corrosion which will destroy the passive layer formed on its surface and lead to successive formation of new oxide layers. This process leads to the formation of wear debris that can be resorbed by the organism and lead to undesired outcomes (Buciumeanu et al., 2018; Runa et al., 2013). Therefore, several studies have been made to improve the tribological response of this material, by applying coatings (Fu et al., 1998; Lee, 2012), performing surface treatments (Dong and Bell, 2000), developing composites (Buciumeanu et al., 2017; Dantas et al., 2017b), etc. In fact, some studies already stated that the addition of these bioactive materials (HAp and βTCP) will enhance the overall microhardness of the component and therefore their wear resistance (Buciumeanu et al., 2017; Dantas et al., 2017b).

In this sense, the present work aims to evaluate the tribological behavior of Ti6Al4V cellular structures impregnated either with HAp and βTCP against an alumina (Al_2O_3) plate and understand its potential for improving the tribological performance of load-bearing implants.

2. Experimental details

2.1. Specimens fabrication

For the present work, Ti6Al4V cellular structures impregnated with bioactive materials (βTCP and HAp) were produced and evaluated.

Ti6Al4V powder purchased from SLM solutions (Germany), with a particle size (d50) of 34 μm, was used to produce Ti6Al4V cellular structures by using SLM technique, with further details on this fabrication being given below. The bioactive materials: βTCP (d50 = 2.26 μm) and HAp (d50 = 10 μm), that were used to impregnate the cellular structures were purchased from Trans-Tech, Inc. and Fluidinova S.A. (nanoXim. Hap203®), respectively. Fig. 1 displays SEM micrographs of Ti6Al4V, βTCP and HAp powders.

As presented in Table 1, the three groups of specimens tested in this study are based in SLM-produced cellular structures. These structures were previously designed on a CAD software and fabricated on a Selective Laser Melting equipment from *SLM Solutions* (model 125HL). Briefly, the CAD data were imported to the SLM software that slices the part in successive layers that will be further scanned by a laser and, layer-by-layer, produce the final component. Based on previous optimization studies for this alloy (Bartolomeu et al., 2017, 2016), the specimens were produced by SLM using the following processing
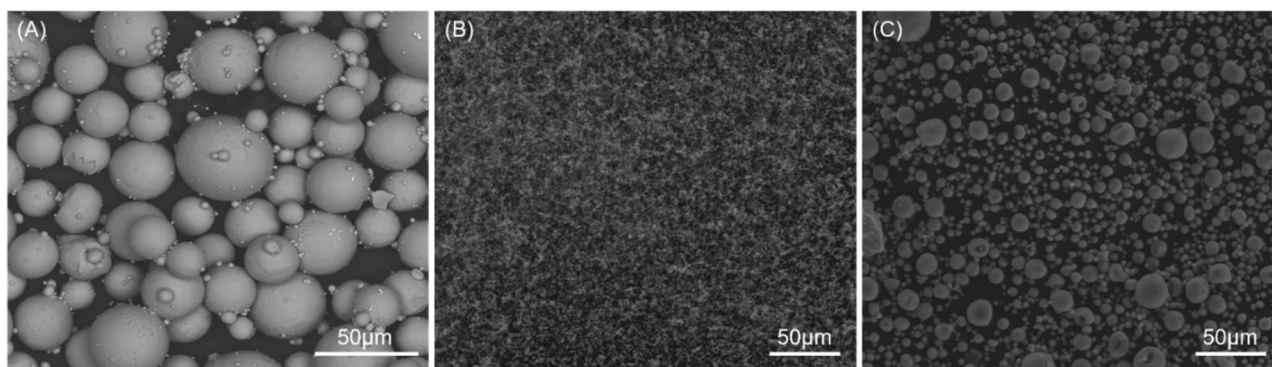

Fig. 1. SEM micrographs of (A) Ti6Al4V, (B) βTCP and (C) HAp powders.

Table 1

Ti6Al4V-based specimens' schematic representation, group number, description and fabrication method.

Representation	Group number	Description	Fabrication method
	G1	Ti6Al4V cellular structure	Selective Laser Melting
	G2	Ti6Al4V cellular Structure impregnated w/ βTCP	Selective Laser Melting + press and sintering
	G3	Ti6Al4V cellular structure impregnated w/ HAp	Selective Laser Melting + press and sintering

Fig. 3. Schematic representation of tribological test.

2.2. Tribological tests

Once prepared, the specimens from the three groups were subjected to flat-on-flat (FOF) reciprocating sliding tests, in which the counterpart was an alumina (Al$_2$O$_3$) plate (50 × 25 × 5 mm), performed in a Bruker-UMT-2 (USA) tribometer (Fig. 3(B)). The whole apparatus of the tests performed in this study is schematically represented in Fig. 3(A).

The alumina plate was polished with resin bonded diamond grinding discs (*MD-Piano 120 and 220*), displaying an Ra of 0.869 ± 0.024 μm.

The specimens were placed in a metallic support that in turn is attached to the load cell. On the other hand, the alumina plate was fixed to an acrylic container that is also fixed to the oscillatory plate of the tribometer. To obtain an approximation of the physiological conditions, the whole apparatus is immersed in a phosphate buffer saline (PBS) solution and an oscillating frequency of 1 Hz was selected.

Taylor et al. (1995) reported that compressive radial stresses starting from 2 MPa can be generated in the bone during the press-fit. To replicate these conditions, in the experimental tests performed in this study, Ti6Al4V specimens having a diameter of 6 mm (surface area ~ 28 mm^2) were used against alumina plate under a normal load of 50 N, thus corresponding to a stress of approximately 2 MPa.

Each test was performed in four iterations, that were named in this paper as static initial (Si), implantation (I), final static (Sf) and tribological performance (Tp).

The first three iterations aim to mimic the moment of implantation/insertion of an implant, while the last one aims to evaluate the tribological performance in terms of mass loss of the specimens (Tp test).

In other words, during the implantation, for instance of hip implants, the ill femoral head, neck and acetabulum is removed from the patient and replaced by the prosthesis. Afterwards, at the time of the

parameters: laser power: 90 W; scan speed: 600 mm/s; scan spacing: 80 μm; layer thickness: 30 μm.

These structures were designed to have a pore size and wall thickness of 400 μm, with interconnected porosity. The produced scaffolds displayed an average thickness of 2.5 mm and 6 mm in diameter.

The non-reinforced scaffolds were tested, being referred along this study as G1.

For producing G2 and G3 groups, a batch of samples produced in the same way as G1 were used to impregnate the bioactive materials. The impregnation process begins by preparing a viscous solution that contains either βTCP or HAp and acetone. Afterwards, the cellular structures were positioned inside a steel mold with 10 mm diameter where the introduction of the bioactive solution is then made by applying pressure using a hydraulic press for 10 min. Finally, the samples were removed from the steel mold and sintered in an induction heated chamber under vacuum at 1100 °C and kept at this temperature for 2 h. Fig. 2 displays a schematic representation of the specimens' production from its SLM process until the impregnation of the bioactive materials.

Finally, after their production, the samples from all the three groups were polished using abrasive silicon carbide papers from P120 until P4000 and ultrasonically cleaned with isopropanol.
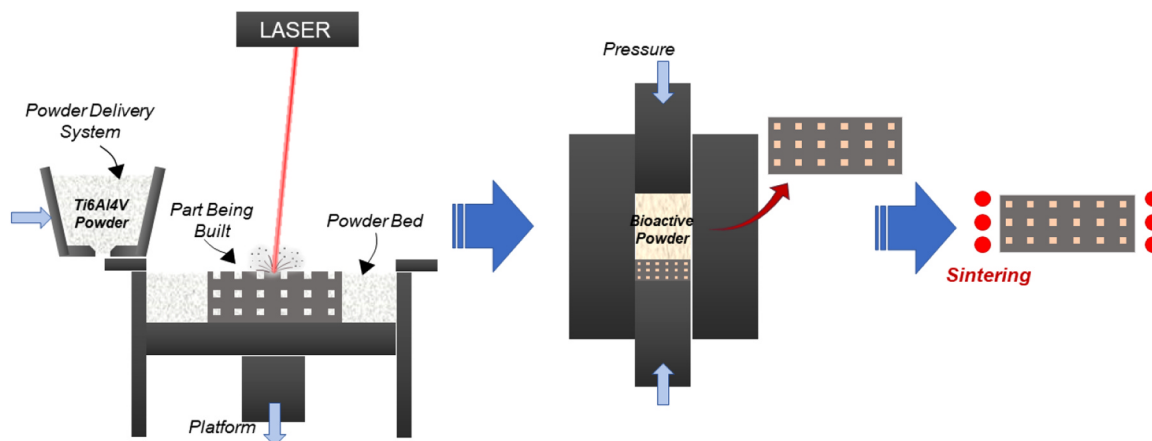

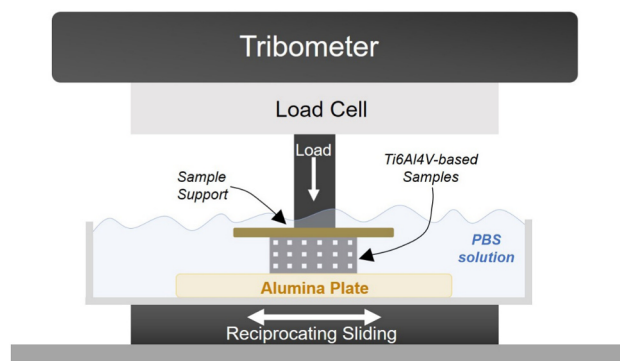**Fig. 2.** Schematic representation of the specimens' production.

prosthesis implantation, there is an initial opposing force to the movement of the implant (frictional force) – this phenomenon was reproduced by the so called static initial (Si) test.

When the surgeon inserts the implant into the bone cavity, an interaction between implant and bone will occur, being this aspect assessed by the implantation (I) test. This test was performed for a stroke length of 3 mm and a total sliding distance of 51.6 mm.

After the implant reaches its final position, there is a final opposing force which dictates the final stability of the implant relative to the bone (commonly referred in literature as primary stability (Affatato, 2014; Dantas et al., 2017a; Moura et al., 2017)) which will be assessed by the third test, named final static (Sf).

Tp test, a reciprocating sliding test, that aims to evaluate the mass loss of each specimen, was performed for a stroke length of 3 mm and a total sliding distance of 5400 mm, with a maximum speed of 9,42 mm/s, for a total test time of 30 min.

Each test was performed, as mentioned, under a load of 50 N at 1 Hz in which the stroke length was 3 mm that in turn corresponds to a total sliding distance for I and Tp of 51.6 mm and 5400 mm, respectively. It is important to highlight that for each group, in average three specimens were analyzed, being the results displayed as the average of those repetitions.

2.3. Specimens characterization: Weight loss calculation, roughness measurement and SEM/EDS analysis

The specimens' roughness before the tribological tests was measured on *Mitutoyo Surftest SJ-210 series* roughness equipment.

Before and after the tribological tests, three measurements of the mass of each sample were made in a *Mettler AE 240* balance (sensitivity of 40 g at a readability of 0.01 mg), to obtain a mean of the weight loss of each group.

The microstructure of the produced specimens' surface after and before the tribological tests and also the morphology of the worn surfaces was assessed by means of Scanning Electron Microscopy (SEM).

Additionally, the alumina plate was also analyzed in order to assess the material transfer to the counterpart during sliding. In this sense, chemical characterization on the alumina plate and some sites of the cellular structures worn surfaces was made by Energy-dispersive X-ray spectroscopy analysis (EDS).

3. Results and discussion

3.1. Specimens characterization

In the present study, Ti6Al4V cellular structures were produced by SLM and impregnated with bioactive materials by using press and sintering technique. Fig. 4 displays the morphology of the Ti6Al4V-based specimens (G1, G2 and G3) before the tribological tests. These specimens contacting surfaces have been polished and the average
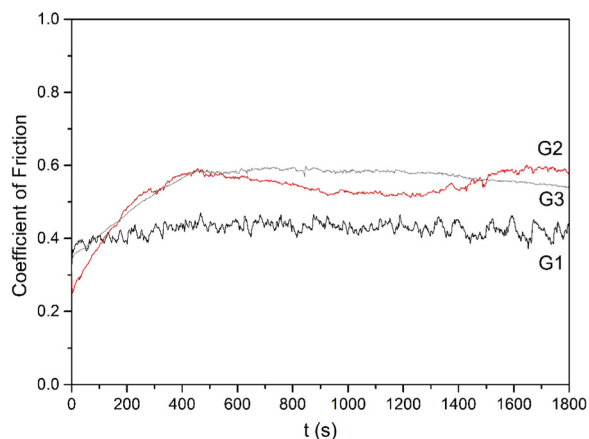

Fig. 5. Coefficient of friction evolution for the tested Ti6Al4V-based specimens against alumina plate.

Table 2
Coefficient of friction values obtained for Tp (Tribological performance) test.

Material	Coefficient of friction	
	Average	SD
G1	0.441	0.015
G2	0.561	0.030
G3	0.477	0.052

roughness of the metallic walls was measured. No statistically significant differences were found between all the groups (e.g. the measured Ra for G1 (non-reinforced specimens) was 0.176 ± 0.036 μm and for G2 was 0.095 ± 0.035 μm).

From Fig. 4 it is possible to observe that all the groups exhibit similar surface morphology. Moreover, it is notable that the pore size of the manufactured specimens is smaller than the CAD designed dimension, an inherent aspect of this additive manufacturing technology, abundantly reported by other authors (Bartolomeu et al., 2017; Taniguchi et al., 2016), mainly due to powder related aspects (size distribution) and to the over melting beyond the laser path (related with thermal conductivity).

By analyzing Fig. 4(B) and (C) it is possible to validate the impregnation process of the bioactive materials. By comparing these two images (Fig. 4(B) and (C)), βTCP-impregnated specimens (G2) seem to present a higher filling of the pores than HAp-impregnated ones (G3). This fact may be related with the particle size of HAp, that is higher (d50 = 10 μm) than βTCP (d50 = 2.26 μm). In fact, it is reported in literature that the packing density is highly dependent on particle size distribution in which a smaller particle size of the powder will lead to a
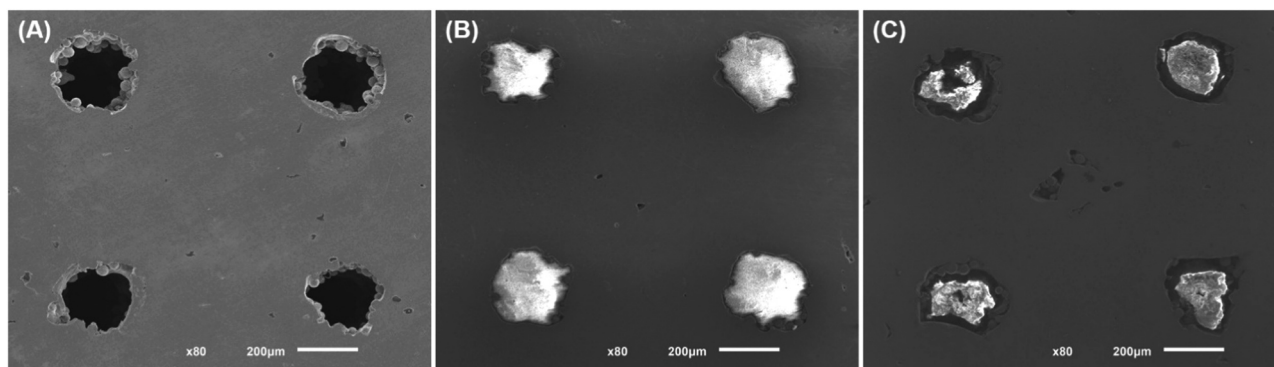

Fig. 4. SEM micrographs of the surfaces of the produced Ti6Al4V-based specimens (A) G1, (B) G2 and (C) G3.
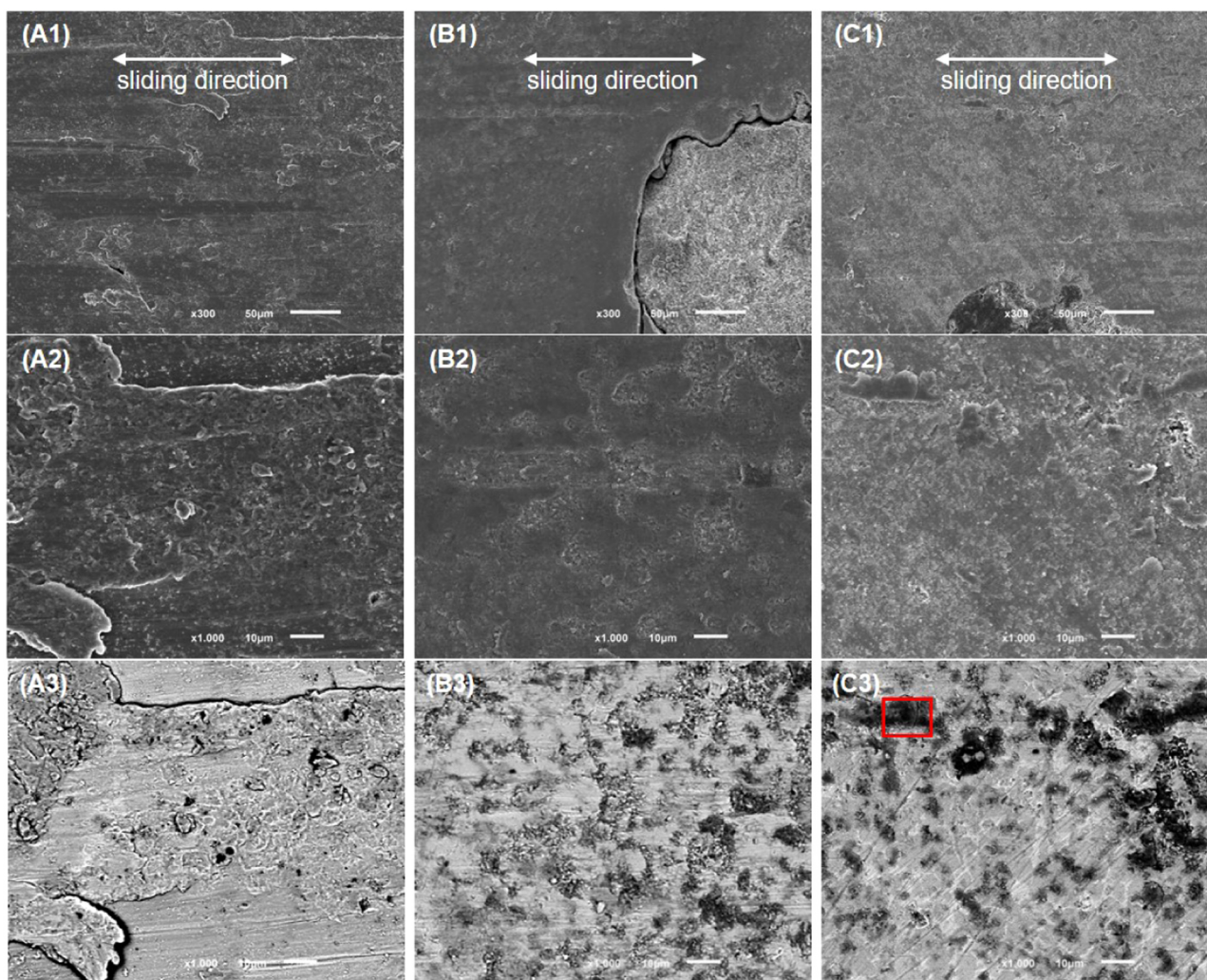
Fig. 6. SEM micrographs of the worn Ti6Al4V-based specimens against alumina: (A), (B) and (C) are G1, G2 and G3 in which 1, 2 and 3 are micrographs at higher magnification, lower and backscattered mode, respectively, with marked area where EDS analysis was performed.

Table 3
Weight loss obtained for G1, G2 and G3 against alumina plate.

Material	Weight Loss (mg)	
	Average	SD
G1	0.921	0.088
G2	0.668	0.122
G3	0.732	0.174

smoother surface finishing with lower porosity and, therefore, a higher densification (German, 2005; Pease III and West, 2002). Therefore, the impregnation process is more difficult to achieve when using a higher particle size.

3.2. Tribological behavior

3.2.1. Tribological performance (Tp) test

The evolution of the coefficient of friction on the Ti6Al4V-based structures during tribological performance (Tp) test is displayed in Fig. 5. For the three groups tested, coefficient of friction curves follows a typical evolution once this value quickly increases in the beginning (more pronounced on G1), before reaching a steady-state regime. This steady-state regime presents some oscillations, more evident on G1, attributable to the material transfer from Ti6Al4V to the alumina plate

and to the third body effect phenomenon.

By analyzing the average coefficient of friction values (Table 2) it is possible to observe that the presence of these harder bioactive materials (6.1 GPa (Boilet et al., 2013) for HAp and 4.9 GPa (Boilet et al., 2013) for βTCP) led to a coefficient of friction increase, when compared to un-reinforced Ti6Al4V ($\approx$ 3.8 GPa) (Bartolomeu et al., 2016)), as reported in other studies (Buciumeanu et al., 2017; Dantas et al., 2017b).

As seen in Fig. 6, after sliding against the alumina plate (Tp test) it is noticeable the detachment of bioactive material (either βTCP or HAp) from the pores of the structure. Then these harder materials are transferred to the metallic walls, where they remain adhered. Due to this fact, the sliding between the bioactive (either βTCP or HAp) and the alumina plate will have a predominant contribution to the coefficient of friction. In literature, the coefficient of friction between βTCP and alumina is commonly reported around 0.90 (Elghazel et al., 2018; Trabelsi et al., 2019), while the coefficient of friction between HAp and alumina is reported in the range 0.70–0.85 (Kalin et al., 2002). Both of these values are substantially above the coefficient of friction between Ti6Al4V and alumina (measured result of 0.441). Despite the higher hardness of these bioactive materials, these facts can explain the higher coefficient of friction found for G2 group, followed by G3, when compared with G1 (see Table 2).

By analyzing the different weight losses obtained by the different groups (Table 3) some differences between them are found, with G1 displaying the higher weight loss and, therefore, the worst wear
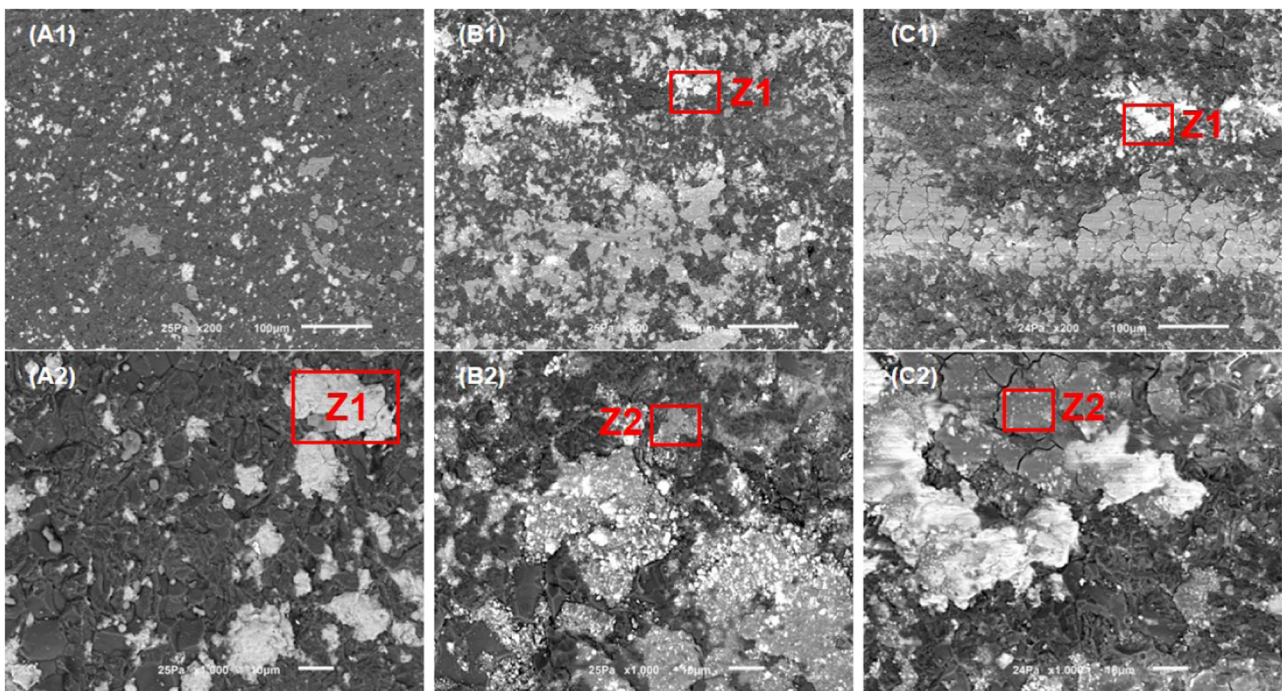
Fig. 7. SEM micrographs of the counterpart (Al_3O_2 plate) worn surface subjected to tribological tests against (A) G1, (B) G2 and (C) G3. Each marked zone corresponds to the different material transferred to the Al_3O_2.

Table 4
Chemical composition (in wt%) of the material transfer zones in Al_3O_2 plate.

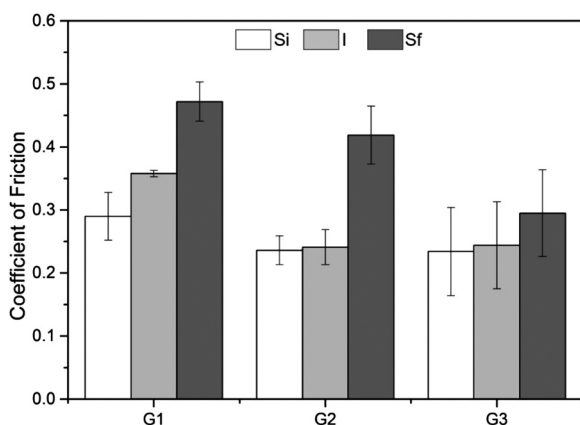| Composition, wt%	G1	G2		G3	
	Z1	Z1	Z2	Z1	Z2
Ti	52.3	50.2	30.7	41.0	20.9
Al	12.1	13.4	12.5	10.7	9.8
V	1.7	2.8	1.1	1.7	1.0
Ca	–	0.2	1.5	–	0.7
P	0.7	0.7	4.2	1.9	7.9
O	29.0	27.4	42.6	37.1	52.8
Na	0.7	0.3	1.3	0.8	2.9
K	–	–	0.8	0.4	2.0
C	2.8	5.0	5.0	6.2	1.7
Cl	0.6	–	0.2	0.1	0.3

Fig. 8. Mean values of coefficient of friction obtained on the tested Ti6Al4V-based specimens.

resistance, while G2 displayed the lower weight loss.

In fact, among these groups, G1 displayed the worse performance (higher weight loss), fact that could be related with the higher contact

pressure involved during the test, once for G1 the same load is applied in a smaller area, when compared with the other groups in which the cells are filled with bioactive materials.

When comparing Ti6Al4V cellular structures impregnated with hydroxyapatite (G3) with the non-impregnated structures (G1), a 20.5% decrease on weight loss was found. Following the same trend, Ti6Al4V cellular structures impregnated with βTCP (G2) displayed an even higher reduction on their weight loss, in the order of 27.4%, when compared to G1.

The wear surfaces after Tp tribological performance tests against alumina plate are visible in Fig. 6 while SEM micrographs of the alumina plate can be seen in Fig. 7. Regarding the wear mechanisms, by analyzing Fig. 6, it is possible to observe in all the Ti6Al4V-based specimens the presence of abrasive grooves which are aligned with the sliding direction. In the images at higher magnification (Fig. 6A2, B2 and B3) the presence of worn areas indicating plastic deformation resulting from the rubbing movements are visible, as well as the release of wear debris.

In G1 specimens (Fig. 6A) the abrasion is more pronounced that on specimens from other groups (Fig. 6B and C) once, as mentioned, the bioactive material will protect the metallic surface from wear. Moreover, delamination is clearly seen due to the formation of plate-like metallic fragments during sliding (Sahoo et al., 2014; Singh and Alpas, 1996). Delamination wear mechanism occurs when large local strains are generated at layers adjacent to the contact surface and wear proceeds by mechanisms such as subsurface delamination (Singh and Alpas, 1996). Also for G1 group, by analyzing the counterpart SEM micrographs (Fig. 7(A)) and EDS results (Table 4), it is also possible to observe adhesion mechanism, once Ti6Al4V was transferred to the alumina plate.

G2 and G3 specimens wear surfaces are shown in Fig. 6(B) and (C) respectively, both having a similar appearance, with a smoother wear track than that of G1. This topographical difference and also the weight loss decrease found for the bioactive-impregnated structures – G2 and G3 (Table 3), can be justified by these harder particles protecting role to the softer material (Ti6Al4V), by supporting the load during sliding (see Fig. 6) (Buciumeanu et al., 2017).

From G3 micrographs at higher magnification (Fig. 6(C3)) it is possible to detect HAp dragged from the open-cells to the Ti6Al4V surface (walls). This is proven by the atomic contrast differences and EDS analysis made on this dragged material (in wt%, 43.9 O; 38.4 Ti; 5.8 Al; 3.9 V; 3.0 P; 0.5 Ca; 4.6 other) and by its brittle nature proven by the presence of cracks (Fig. 6(C2)).

G2 displayed a similar outcome, with βTCP being dragged to Ti6Al4V walls, as proven by the atomic contrast (Fig. 6(B3)), although undetected by EDS analysis, probably due to the lower amount of βTCP transferred to Ti6Al4V walls when compared with HAp specimens.

When looking at Fig. 7(B) and (C) it is possible to identify an expressive material transfer from the specimens to the alumina plates (adhesion wear mechanism), for both G2 and G3 groups. From these images and Table 3 results it is possible to conclude that besides titanium alloy transfer, also bioactive material was found adhered to the plate. This phenomenon is more evident in G3 than G2, once a higher amount of transfer material was generally found for the previous, displaying several cracks, suggesting the brittle nature of this transferred tribolayer (Kalin et al., 2002).

3.2.2. Initial and final static coefficient and implantation tests

Fig. 8 presents the average coefficient of friction of the first three tribological tests performed for the three groups.

The first test (Si), as previously mentioned, corresponds to the initial opposing force to the movement of the implant. The results for this test showed very similar static coefficient of friction, for all the groups (Fig. 8). This outcome seems to indicate that during these first seconds (that encompass the Si test) no detachment of the bioactive occurred due to its mechanical interlocking inside these structures open-cells. Furthermore, these results may indicate that for G2 and G3, the metal is dictating the initial opposing force to motion, since Ti6Al4V area is expressively higher than that of the bioactives.

of friction that is more pronounced in Sf tests. These results indicate that there is a good adhesion between these specimens and the alumina plate.

4. Conclusions

Ti6Al4V cellular structures impregnated with βTCP or HAp were designed and produced by using an Additive Manufacturing technique (SLM) combined with press and sintering. These multi-material structures assure no detachment of the bioactive material by using a mechanical interlocking strategy. These multi-functional structures will enhance the interaction between bone and implant, by promoting bone ingrowth into the structures open-cells as the bioactive material is being absorbed and replaced by newly formed bone.

The introduction of bioactive materials inside these SLM-fabricated Ti6Al4V structures led to an increased wear performance, with a weight loss decrease of 27.4% for βTCP- Ti6Al4V structures and 20.5% for HAp-Ti6Al4V structures, when compared to unreinforced structures.

The proposed solution is a promising approach by gathering suitable mechanical properties (strength and stiffness) for load-bearing implants, assured by the metallic structure; bioactive properties, assured by the bioactive materials and in addition an improved wear performance by introducing these bioactive materials.

The second test (I) intends to reproduce the insertion course of the implant into the bone cavity. Comparing the static initial coefficient (Si) and the dynamic coefficient (I), no significant differences were observed between them (Fig. 8), which is in accordance with literature that states that the static coefficient of friction values are higher or equal to the kinetic coefficient of friction (Bhushan, 2013; Moura et al., 2017). Regarding the comparison between the final coefficient of friction (Sf) and the dynamic coefficient (I), greater values were found for the previous, again in line with literature (Bhushan, 2013; Moura et al., 2017).

The final static coefficient (Sf) is extremely important to assess the primary stability of bone, once a higher coefficient of friction will guarantee that, after implantation, there is a good adhesion between bone and the implant material. The results obtained in this study show that G2, that displayed the highest wear resistance (Tribological performance test) revealed one of the highest static coefficient of friction (Sf) (Fig. 8), making this material a good option for improved primary stability.

When talking about friction, and according to Bowden and Tabor theory, the total frictional force is a sum of the adhesion force between two surfaces and the deformation force of the same surfaces (Bhushan, 2013; Bowden and Tabor, 1964). The performed tests show that Sf test coefficient of friction values are much higher than those of Si, for all groups, being this difference associated with the adhesion component

References

Affatato, S., 2014. Perspectives in total hip arthroplasty - advances in biomaterials and their tribological interactions. Biomaterials. https://doi.org/10.1016/B978-1-78242-031-6.50016-7.

Aparicio, C., Padrós, A., Gil, F.J., 2011. In vivo evaluation of micro-rough and bioactive titanium dental implants using histometry and pull-out tests. J. Mech. Behav. Biomed. Mater. 4, 1672–1682. https://doi.org/10.1016/j.jmbbm.2011.05.005.

Apostu, D., Lucaciu, O., Berce, C., Lucaciu, D., Cosma, D., 2017. Current methods of preventing aseptic loosening and improving osseointegration of titanium implants in cementless total hip arthroplasty: a review. J. Int. Med. Res. 0. https://doi.org/10.1177/0300060517732697.

Arabnejad, S., Burnett Johnston, R., Pura, J.A., Singh, B., Tanzer, M., Pasini, D., 2016. High-strength porous biomaterials for bone replacement: a strategy to assess the interplay between cell morphology, mechanical properties, bone ingrowth and manufacturing constraints. Acta Biomater. 30, 345–356. https://doi.org/10.1016/j.actbio.2015.10.048.

Bandyopadhyay, A., Espana, F., Balla, V.K., Bose, S., Ohgami, Y., Davies, N.M., 2010. Influence of porosity on mechanical properties and in vivo response of Ti6Al4V implants. Acta Biomater. 6, 1640–1648. https://doi.org/10.1016/j.actbio.2009.11.011.

Bartolomeu, F., Faria, S., Carvalho, O., Pinto, E., Alves, N., Silva, F.S., Miranda, G., 2016. Predictive models for physical and mechanical properties of Ti6Al4V produced by selective laser melting. Mater. Sci. Eng. A 663, 181–192. https://doi.org/10.1016/j.msea.2016.03.113.

Bartolomeu, F., Sampaio, M., Carvalho, O., Pinto, E., Alves, N., Gomes, J.R., Silva, F.S., Miranda, G., 2017. Tribological behavior of Ti6Al4V cellular structures produced by selective laser melting. J. Mech. Behav. Biomed. Mater. 69, 128–134. https://doi.org/10.1016/j.jmbbm.2017.01.004.

Bhushan, B., 2013. Principles and Applications of Tribology, 2nd ed. John Wiley & Sons,

Ltd., USA. https://doi.org/10.1002/9781118403020.

Blind, O., Klein, L.H., Dailey, B., Jordan, L., 2005. Characterization of hydroxyapatite films obtained by pulsed-laser deposition on Ti and Ti-6AL-4v substrates. Dent. Mater. 21, 1017–1024. https://doi.org/10.1016/j.dental.2004.12.003.

Bobyn, J.D., Pilliar, R.M., Cameron, H.U., Weatherly, G.C., 1980. The optimum pore size for the fixation of porous-surfaced metal implants by the ingrowth of bone. Clin. Orthop. Relat. Res. 263–270.

Boilet, L., Descamps, M., Rguiti, E., Tricoteaux, A., Lu, J., Petit, F., Lardot, V., Cambier, F., Leriche, A., 2013. Processing and properties of transparent hydroxyapatite and β tricalcium phosphate obtained by HIP process. Ceram. Int. 39, 283–288. https://doi.org/10.1016/j.ceramint.2012.06.023.

Bowden, F.P., Tabor, D., 1964. The Friction and Lubrication of Solids. Clarendon Press, Oxford, UK.

Bruschi, S., Bertolini, R., Ghiotti, A., 2017. Coupling machining and heat treatment to enhance the wear behaviour of an Additive Manufactured Ti6Al4V titanium alloy. Tribol. Int. 116, 58–68. https://doi.org/10.1016/j.triboint.2017.07.004.

Buciumeanu, M., Almeida, S., Bartolomeu, F., Costa, M.M., Alves, N., Silva, F.S., Miranda, G., 2018. Ti6Al4V cellular structures impregnated with biomedical PEEK - new material design for improved tribological behavior. Tribol. Int. 119. https://doi.org/10.1016/j.triboint.2017.10.038.

Buciumeanu, M., Araujo, A., Carvalho, O., Miranda, G., Souza, J.C.M., Silva, F.S., 2017. Study of the tribocorrosion behaviour of Ti6Al4V – HA biocomposites. Tribiol. Int. 107, 77–84. https://doi.org/10.1016/j.triboint.2016.11.029.

Dantas, T.A., Abreu, C.S., Costa, M.M., Miranda, G., Silva, F.S., Dourado, N., Gomes, J.R., 2017a. Bioactive materials driven primary stability on titanium biocomposites. Mater. Sci. Eng. C 77, 1104–1110. https://doi.org/10.1016/j.msec.2017.04.014.

Dantas, T.A., Costa, M.M., Miranda, G., Silva, F.S., Abreu, C.S., Gomes, J.R., 2017b. Effect of HAp and β-TCP incorporation on the tribological response of Ti6Al4V biocomposites for implant parts. J. Biomed. Mater. Res. Part B Appl. Biomater. 1–7. https://doi.org/10.1002/jbm.b.33908.

Dong, H., Bell, T., 2000. Enhanced wear resistance of titanium surfaces by a new thermal oxidation treatment. Wear 238, 131–137. https://doi.org/10.1016/S0043-1648(99)00359-2.

Ducheyne, P., Qiu, Q., 1999. Bioactive ceramics: the effect of surface reactivity on bone formation and bone cell function. Biomaterials 20, 2287–2303. https://doi.org/10.1016/S0142-9612(99)00181-7.

Elghazel, A., Taktak, R., Elleuch, K., Bouaziz, J., 2018. Mechanical and tribological properties of tricalcium phosphate reinforced with fluorapatite as coating for orthopedic implant. Mater. Lett. 215, 53–57. https://doi.org/10.1016/j.matlet.2017.12.044.

Evis, Z., Doremus, R.H., 2007. Hot-pressed hydroxylapatite/monoclinic zirconia composites with improved mechanical properties. J. Mater. Sci. 42, 2426–2431. https://doi.org/10.1007/s10853-006-1299-6.

Fu, Y., Batchelor, A.W., Wang, Y., Khor, K.A., 1998. Fretting wear behaviors of thermal sprayed hydroxyapatite (HA) coating under unlubricated conditions. Wear 217, 132–139. https://doi.org/10.1016/S0043-1648(98)00142-2.

German, R.M., 2005. Powder Metallurgy & Particulate Materials Processing, Metal Powd. ed. Princeton.

Horowitz, R. a., Ziv, D.D.S., Dmd, M., Foitzik, C., Prasad, H., Rohrer, M.D.T.M., Palti, M.S.A., 2009. ß-tricalcium phosphate as bone substitute material: properties and clinical applications. Int. J. Dent. Implant. Biomater. 1, 2–11.

Hu, J., Wang, Z., Guan, T., Gao, Y., Lv, X., Lin, X., Tang, C. yin, Gao, B., 2010. In situ synthesis and fabrication of tricalcium phosphate bioceramic coating on commercially pure titanium by laser rapid forming. Surf. Coat. Technol. 204, 3833–3837. https://doi.org/10.1016/j.surfcoat.2010.04.062.

Kalin, M., Jahanmir, S., Ives, L.K., 2002. Effect of counterface roughness on abrasive wear of hydroxyapatite. Wear 252, 679–685. https://doi.org/10.1016/S0043-1648(02)00028-5.

Karamian, E., Khandan, A., Kalantar Motamedi, M.R., Mirmohammadi, H., 2014. Surface characteristics and bioactivity of a novel natural HA/zircon nanocomposite coated on dental implants. Biomed. Res. Int. 2014. https://doi.org/10.1155/2014/410627.

Khandelwal, H., Singh, G., Agrawal, K., Prakash, S., Agarwal, R.D., 2013. Characterization of hydroxyapatite coating by pulse laser deposition technique on stainless steel 316 L by varying laser energy. Appl. Surf. Sci. 265, 30–35. https://doi.org/10.1016/j.apsusc.2012.10.072.

Kumar, A., Mandal, S., Barui, S., Vasireddi, R., Gbureck, U., Gelinsky, M., Basu, B., 2016. Low temperature additive manufacturing of three dimensional scaffolds for bone-tissue engineering applications: processing related challenges and property assessment. Mater. Sci. Eng. R Rep. 103, 1–39. https://doi.org/10.1016/j.mser.2016.01.001.

Lee, C.-K., 2012. Fabrication, characterization and wear corrosion testing of bioactive hydroxyapatite/nano-TiO2 composite coatings on anodic Ti–6Al–4V substrate for biomedical applications. Mater. Sci. Eng. B 177, 810–818. https://doi.org/10.1016/J.MSEB.2012.03.034.

Lee, D.H., Tripathy, N., Shin, J.H., Song, J.E., Cha, J.G., Min, K.D., Park, C.H., Khang, G., 2017. Enhanced osteogenesis of β-tricalcium phosphate reinforced silk fibroin scaffold for bone tissue biofabrication. Int. J. Biol. Macromol. 95, 14–23. https://doi.org/10.1016/j.ijbiomac.2016.11.002.

Massaro, C., Rotolo, P., De Riccardis, F., Milella, E., Napoli, a., Wieland, M., Textor, M., Spencer, N.D., Brunette, D.M., 2002. Comparative investigation of the surface properties of commercial titanium dental implants. Part I: chemical composition. J. Mater. Sci. Mater. Med. 13, 535–548. https://doi.org/10.1023/A:1015170625506.

Melo-Fonseca, F., Lima, R., Costa, M.M., Bartolomeu, F., Alves, N., Miranda, A., Gasik, M., Silva, F.S., Silva, N.A., Miranda, G., 2018. 45S5 BAG-Ti6Al4V structures: the influence of the design on some of the physical and chemical interactions that drive cellular response. Mater. Des. 160, 95–105. https://doi.org/10.1016/J.MATDES.2018.08.056.

Miranda, G., Araújo, A., Bartolomeu, F., Buciumeanu, M., Carvalho, O., Souza, J.C.M., Silva, F.S., Henriques, B., 2016. Design of Ti6Al4V-HA composites produced by hot pressing for biomedical applications. Mater. Des. 108, 488–493. https://doi.org/10.1016/j.matdes.2016.07.023.

Moura, C.G., Pereira, R., Buciumeanu, M., Carvalho, O., Bartolomeu, F., Nascimento, R., Silva, F.S., 2017. Effect of laser surface texturing on primary stability and surface properties of zirconia implants. Ceram. Int. 43, 15227–15236. https://doi.org/10.1016/j.ceramint.2017.08.058.

Ning, C.Q., Zhou, Y., 2002. In vitro bioactivity of a biocomposite fabricated from HA and Ti powders by powder metallurgy method. Biomaterials 23, 2909–2915. https://doi.org/10.1016/S0142-9612(01)00419-7.

Pease III, L.F., West, W.G., 2002. Fundamentals of Powder Metallurgy. Metal Powder Industry, USA.

Pereira, B.L., Tummler, P., Marino, C.E.B., Soares, P.C., Kuromoto, N.K., 2014. Titanium bioactivity surfaces obtained by chemical/electrochemical treatments. Rev. Mater. 19, 16–23. https://doi.org/10.1590/S1517-70762014000100004.

Queiroz, A.C., Santos, J.D., Vilar, R., Eugénio, S., Monteiro, F.J., 2004. Laser surface modification of hydroxyapatite and glass-reinforced hydroxyapatite. Biomaterials 25, 4607–4614. https://doi.org/10.1016/j.biomaterials.2003.11.054.

Ratner, B.D., Hoffman, A.S., Schoen, F.J., Lemons, J.E., 1996. Biomaterials Science - an introduction to materials in medicine. Biomater. Sci. Introd. Mater. Med. https://doi.org/10.1016/B978-0-08-087780-8.00148-0.

Runa, M.J., Mathew, M.T., Rocha, L.A., 2013. Tribocorrosion response of the Ti6Al4V alloys commonly used in femoral stems. Tribol. Int. 68, 85–93. https://doi.org/10.1016/j.triboint.2013.09.022.

Ryan, G., Pandit, A., Apatsidis, D.P., 2006. Fabrication methods of porous metals for use in orthopaedic applications. Biomaterials 27, 2651–2670. https://doi.org/10.1016/j.biomaterials.2005.12.002.

Sahoo, R., Jha, B.B., Sahoo, T.K., 2014. Dry sliding wear behaviour of Ti-6Al-4V alloy consisting of bimodal microstructure. Trans. Indian Inst. Met. 67, 239–245. https://doi.org/10.1007/s12666-013-0343-x.

Sampaio, M., Buciumeanu, M., Henriques, B., Silva, F.S., Souza, J.C.M., Gomes, J.R., 2016. Tribocorrosion behavior of veneering biomedical PEEK to Ti6Al4V structures. J. Mech. Behav. Biomed. Mater. 54, 123–130. https://doi.org/10.1016/j.jmbbm.2015.09.010.

Santin, M., Philips, G., 2012. Biomimetic, Bioresponsive, and Bioactive Materials - An Introduction to Integrating Materials with Tissues. John Wiley & Sons, USA.

Sidambe, A.T., 2014. Biocompatibility of advanced manufactured titanium implants-a review. Materials 7, 8168–8188. https://doi.org/10.3390/ma7128168.

Singh, J., Alpas, A.T., 1996. High-temperature wear and deformation processes in metal matrix composites. Metall. Mater. Trans. A Phys. Metall. Mater. Sci. 27, 3135–3148. https://doi.org/10.1007/BF02663864.

Tan, X.P., Tan, Y.J., Chow, C.S.L., Tor, S.B., Yeong, W.Y., 2017. Metallic powder-bed based 3D printing of cellular scaffolds for orthopaedic implants: a state-of-the-art review on manufacturing, topological design, mechanical properties and biocompatibility. Mater. Sci. Eng. C 76, 1328–1343. https://doi.org/10.1016/J.MSEC.2017.02.094.

Taniguchi, N., Fujibayashi, S., Takemoto, M., Sasaki, K., Otsuki, B., Nakamura, T., Matsushita, T., Kokubo, T., Matsuda, S., 2016. Effect of pore size on bone ingrowth into porous titanium implants fabricated by additive manufacturing: an in vivo experiment. Mater. Sci. Eng. C 59, 690–701. https://doi.org/10.1016/j.msec.2015.10.069.

Taylor, M., Tanner, K.E., Freeman, M.A.R., Yettram, A.L., 1995. Cancellous bone stresses surrounding the femoral component of a hip prosthesis: an elastic-plastic finite element analysis. Med. Eng. Phys. 17, 544–550. https://doi.org/10.1016/1350-4533(95)00018-I.

Trabelsi, M., AlShahrani, I., Algarni, H., Ben Ayed, F., Yousef, E.S., 2019. Mechanical and tribological properties of the tricalcium phosphate - magnesium oxide composites. Mater. Sci. Eng. C 96, 716–729. https://doi.org/10.1016/j.msec.2018.11.070.

Van Hooreweder, B., Apers, Y., Lietaert, K., Kruth, J.P., 2017. Improving the fatigue performance of porous metallic biomaterials produced by selective laser melting. Acta Biomater. 47, 193–202. https://doi.org/10.1016/j.actbio.2016.10.005.

Zhang, L., He, Z.Y., Zhang, Y.Q., Jiang, Y.H., Zhou, R., 2016. Enhanced in vitro bioactivity of porous NiTi-HA composites with interconnected pore characteristics prepared by spark plasma sintering. Mater. Des. 101, 170–180. https://doi.org/10.1016/j.matdes.2016.03.128.

Zhao, X., Courtney, J.M., Qian, H., 2011. Bioactive materials in medicine - design and applications. Bioact. Mater. Med. Des. Appl. https://doi.org/10.1533/9780857092939.1.